Electronic Supplementary Material (ESI) for Journal of Materials Chemistry C.

Supplementary Information

The Effect of Molecular Aggregation of Thermally Activated Delayed Fluorescence Sensitizer for Hyperfluorescence in Organic Light-Emitting Diodes

Eun Young Park[1], Ji Hyun Park,[2+] ,Yun-Hi Kim*[,2], Min Chul Suh*[,1]

[1]*Department of Information Display, Kyung Hee University, Seoul 02447, Republic of Korea*
[2]*Department of Chemistry and RIGET, Gyeongsang National University, Jinju, 660-701, South Korea*

***Corresponding Author**

ORCID

[1]Min Chul Suh: 0000-0002-1295-1693

Department of Information Display, Kyung Hee University, Seoul 02447, Republic of Korea

*E-mail address: mcsuh@khu.ac.kr.

[2]Yun-Hi Kim: 0000-0001-8856-4414

Department of Chemistry and RIGET, Gyeongsang National University, Jinju 660-701, Republic of Korea

*E-mail address: ykim@gnu.ac.kr.

I. Theory

1.1 Understanding of theoretical calculations using TD-DFT methods.

Recently, many studies have identified the properties of materials through quantum computation.[1] In general, the photophysical properties of a material are determined based on the range-separated (RS) exchange density function.

$$\frac{1}{r_{12}} = \frac{1 - [\alpha + \beta\, erf(\omega r_{12})}{r_{12}} + \frac{\alpha + \beta\, rfc(\omega r_{12})}{r_{12}} \quad \text{(S1)}$$

The equation for r_{12} is expressed as the sum of short-range and long-range, where r_{12} stands for electron-electron Coulomb potential. α and β quantify the contribution of the HF exchange to the full range, or the DFT counterpart. In general, the well-known B3LYP theory does not contain 100% Hartree-Fock (HF) exchange. Therefore, there is a tendency to overestimate the distance dependence of the charge transfer excitation energy. In this paper, simulations are performed with long-range theory to accurately predict the distance dependence. Also, in order to predict accurate values, we need to tune the ω that the material corresponds to the theory and basis set. ω is the square of the sum of HOMO and ionization energy, and the ω value can be determined through the point at which J^2 is minimized.[2-4]

$$J^2 = \sum_{i=0}^{1} \left[\varepsilon_H(N+i) + IP(N+i)\right]^2 \quad \text{(S2)}$$

We can optimize the geometry using the ω values obtained through tuning. Also, The energy equations of each excited state are as follows:[5]

$$E(S_1) = E_{S_1}(S_1 - geometry) - E_{S_0}(S_0 - geometry) \quad \text{(S3)}$$

$$E(T_1) = E_{T_1}(T_1 - geometry) - E_{S_0}(S_0 - geometry) \quad \text{(S4)}$$

$$\Delta E_{ST} = E(S_1) - E(T_1) \quad \text{(S5)}$$

$$\lambda_S = E_{S_1}(T_1 - geometry) - E_{S_1}(S_1 - geometry) \quad \text{(S6)}$$

$E(S_1)$ and $E(T_1)$ represent the adiabatic energy in the excited state, and in the case of ΔE_{ST}, it means the adiabatic energy gap calculated as gas phase energy. Also, λ_S are reorganization energy for S_1 and T_1. After we get the geometry calculation results, we can also predict ISC and RISC constant rate using the equation below by Marcus' theory.[6-7]

$$k = \frac{V^2}{\hbar}\sqrt{\frac{\pi}{k_B T\lambda}} exp\left[-\frac{(\Delta E_{ST}+\lambda)^2}{4k_B T\lambda}\right] \quad \text{(S7)}$$

Where k_B is the Boltzmann constant (8.62 × 10^{-5} eV/K), *T* is Kelvin temperature (298K), V stands for the spin orbital coupling matrix element (SOCME) between S_1 and T_1. We can calculate SOCME at the TD-DFT level through the equation shown below [8]:

$$\langle S_1 \left| \hat{H_{SOC}} \right| T_1 \rangle^2 = \sum_{i=1}^{3} [Re^2 \langle S_1 \left| \hat{H_{SOC}} \right| T_{1,i} \rangle + Im^2 [\langle S_1 \left| \hat{H_{SOC}} \right| T_{1,i} \rangle] \quad \text{(S8)}$$

$\hat{H_{SOC}}$ means SCOME complex number and is divided into real and imaginary numbers. In conclusion, we can understand and predict material properties through simulation.

1.2 Simulation method

We introduced a long-range corrected exchange function [i.e., Perdew-Burke-Ernzerhof exchange functional][9] LC-wPBE to tune the range separation parameter ω divided by the HF exchange integral. The basis set used is 6-31G**. The TD-DFT level was optimized with spin-restricted for the geometry of S_1 with omega values applied. Unlike S_1, the geometry case of T_1 was optimized through spin-unrestricted SCF calculations.[10] In addition, the SOCME calculation was calculated using the PBE0 theory and zero-order regular approximation (ZORA) basis set.

1.3 Photo physical properties.

The time-dependent population ratio equations for the densities of singlet [S_1] and triplet [T_1] excited states is expressed as [11-12]:

$$\frac{d}{dt}\left(\frac{[S_1]}{[T_1]}\right) = \begin{pmatrix} -(k_r^S + k_{nr}^S + k_{ISC}) & k_{RISC} \\ k_{ISC} & -(k_r^T + k_{nr}^T + k_{RISC}) \end{pmatrix}\left(\frac{[S_1]}{[T_1]}\right) \quad \text{(S9)}$$

k_r^S and k_{nr}^S are the rate constant about singlet radiative and non-radiative decay from S_1 to S_0 (fluorescence), respectively. Also, k_r^T and k_{nr}^T are the rate constant about triplet radiative and non-radiative decay from T_1 to S_0 (phosphorescence), respectively. The PL quantum efficiencies (Φ_{PLQY}) value expressed as the sum of the prompt (Φ_{PF}) and delayed (Φ_{DF}) components is important in calculating the rate constant of the TADF materials, and each equation is expressed as follows:

$$\Phi_{PF} = \frac{k_r^S}{k_r^S + k_{nr}^S + k_{ISC}} \text{ (S10)}$$

$$\Phi_{DF} = \Phi_{PF} \sum_{k=1}^{\infty} (\Phi_{ISC}\Phi_{RISC})^k = \Phi_{PF} \frac{\Phi_{ISC}\Phi_{RISC}}{1 - \Phi_{ISC}\Phi_{RISC}} \text{ (S11)}$$

Combining **Eq. (S9)-(S11)**, we can calculate the rate constants for the k_{PF} and k_{DF} lifetime of TADF materials.

$$k_{PF} = k_r^S + k_{nr}^S + k_{ISC} = \frac{1}{\tau_{PF}} \text{ (S12)}$$

$$k_{DF} = k_r^T + k_{RISC}(1 - \frac{k_{ISC}}{k_r^S + k_{nr}^S + k_{ISC}}) = \frac{1}{\tau_{PF}} \text{ (S13)}$$

$$\Phi_{ISC} = \frac{k_{ISC}}{k_r^S + k_{nr}^S + k_{ISC}} \text{ (S14)}$$

Eq. (S12)-(S13) are maintained only when the doping concentration is not related to self-quenching, and according to Kim et al.,[13] the equation of concentration quenching rate k_{CQ} can be expressed as:

$$k_{CQ} = k_{DF} + k_{nr}^T - (1 - \Phi_{ISC})k_{RISC} \text{ (S15)}$$

where Φ_{RISC} could be express as:

$$\Phi_{RISC} = \frac{k_{RISC}}{k_{nr}^{T} + k_{RISC} + k_{CQ}} \quad \text{(S16)}$$

II. Experimental

2.1. Instruments.

^{1}H NMR (Proton nuclear magnetic resonance) data were recorded using a Bruker DRX 300 MHz spectrometer. ^{13}C NMR (Carbon nuclear magnetic resonance) data were recorded using a Bruker DRX 500 MHz spectrometer. The thermal analysis measurements were performed using a TA 2050 TGA thermogravimetric analyzer under nitrogen condition at a heating rate of 10 °C/min form 0 °C to 800 °C. Differential scanning calorimetry was conducted under nitrogen at a heating 10 °C/min from 0 °C to 300 °C using a TA Instruments 2100 DSC. Absorption spectra were obtained in toluene using a Shimadzu's UV-3600 UV-Vis-NIR spectrophotometer. Cyclic voltammetry (CV) was measured using an epsilon E3 at room temperature in a 0.1M solution of TBAP in DMF. A three-electrode system was used, composing of a glassy carbon working electrode, a platinum wire counter electrode, and Ag/AgCl reference electrode.

2.2. Device fabrication

Indium tin oxide (ITO) patterned by the photo-lithography process has an active area of 3 x 3 mm^2. We cleaned the ITO substrates with acetone and isopropyl alcohol (IPA) for 10 min, followed by UV-ozone treatment for 15 min to increase adhesion. The CH8000 used as the HIL was spin-coated on an ITO substrate at 10,000 rpm for 22 s. The spin-coated glass was then transferred to an N_2-filled glove box and annealed at 160 °C for 20 min. Afterwards, all HTL and ETL materials were deposited at ~0.5 Å/s. Also, in the case of EML, as an experiment to confirm concentration quenching, DPEPO was doped with DMAC-DPS and Ph-OBNA at 10 wt% ~ 80 wt%, respectively. After the quenching effect experiment, fluorescent dopants were deposited at 1wt% to confirm the spectrum overlap effect for F$\ddot{o}$rster energy transfer. Finally, LiF and Al were deposited at 0.2 Å/s and 3.0 Å/s, respectively. All depositions were performed under 10^{-7} Torr pressure.

2.3. Measurements

Absorption and photo luminescence (PL) properties of materials were measured by UV-vis spectrometer (JASCOV-570, JASCO) and PL spectrophotometer (V-8500, JASCO), respectively. Current density (*J*)-voltage (*V*)-luminance (*L*) (*J*-*V*-*L*) results were obtained through a power supply (SMU 2635A, Keithley) and a luminance meter (CS-100A, Minolta). Also, Electroluminescence (EL) spectra and color coordinates (Commission Internationale de l'Eclairage, for CIE 1931) were measured by using Minolta's CS-2000A spectroradiometer.

The transient PL decay characteristics of the material were measured by a Quantaurus-Tau fluorescence lifetime measurement system (C11367-03, Hamamatsu Photonics), and the excitation energy was fixed at 340 nm LED. In addition, a Quantaurus-QY C11347 (Hamamatsu Photonics, Japan) instrument was used to obtain absolute photoluminescence quantum yield (PLQY) measurements.

2.4. Materials.

Heraeus Clevios™ PVP (CH 8000) was used as the hole injection layer (HIL) material and was purchased from Heraeus. Also, 1,1-*bis*[(di-4-tolylamino)phenyl]cyclohexane (TAPC) and *N*,*N*′-dicarbazolyl-3,5-benzene (mCP) used as the hole transport layer (HTL) were purchased from Lumtec Corp. We used bis[2-(diphenylphosphino)phenyl] ether oxide (DPEPO) as the host in the emitting layer (EML) and purchased from Ossila. Bis[4-(9,9-dimethyl-9,10-dihydroacridine)phenyl]sulfone (DMAC-DPS), a TADF material used as the sensitizer, was purchased from Sigma-Aldrich, and 11-phenyl-11*H*-9,16-dioxa-11-aza-4b-boraindeno[1,2-a]naphtho[3,2,1-de] anthracene (Ph-OBNA) was synthesized as a TADF material, too. Besides, the fluorescent blue dopant 2,5,8,11-tetra-tert-butylperylene (TBPe) was purchased from Lumtec Corp. and used for the hyper fluorescent OLED fabrication. In addition, diphenyl[4-(triphenylsilyl)phenyl]phosphine oxide (TSPO1) and 2,2',2"-(1,3,5-benzinetriyl)-tris(1-phenyl-1-*H*-benzimidazole) (TPBI) were used as exciton blocking layer (EBL) and electron transfer layer (ETL), respectively. In addition, lithium fluoride (LiF) and aluminum (Al) were used as electron injection layer (EIL) and cathode. TSPO1, TPBI, LiF and Al materials used in this study were purchased from Sigma-Aldrich.

2.5. Synthesis of 11-phenyl-11*H*-9,16-dioxa-11-aza-4b-boraindeno[1,2-a]naphtho[3,2,1-de] anthracene (Ph-OBNA).

All chemicals and solvent were purchased form TCI, Alfa aesar and Aldrich. All reagent purchased commercially were used without further purification. $Pd_2(dba)_3$ was purchased from Umicore. In addition, synthesis, NMR information of (1)~(5) and device information can be found in Supporting information. (**Figure S1~S11**)

Synthesis of 8-bromo-5,9-dioxa-13b-boranaphtho[3,2,1-de]anthracene (1) The reaction was followed by literature methods.[14] ^{1}H NMR (300 MHz, CD_2Cl_2) δ = 8.64 (d, J=7.6Hz, 1H) 7.94-7.91 (d, J=8.7Hz, 1H), 7.73-7.64 (m, 2H), 7.59-7.56 (d, J=8.4Hz, 1H), 7.49-7.46 (d, J=8.4Hz, 1H), 7.40-7.32 (m, 2H), 7.12-7.09 (m, 1H).

Synthesis of 4,4,5,5-tetramethyl-2-(2-nitrophenyl)-1,3,2-dioxaborolane (2) The reaction was followed by literature methods.[15] ^{1}H NMR (300 MHz, CD_2Cl_2) δ = 8.19-8.16 (dd, J=1.0Hz, J=8.6Hz, 1H), 7.75-7.70 (m, 1H), 7.63-7.57 (m, 2H), 1.43 (s, 12H).

Synthesis of 8-(2-nitrophenyl)-5,9-dioxa-13b-boranaphtho[3,2,1-de]anthracene (3) 8-Bromo-5,9-dioxa-13b-boranaphtho[3,2,1-de]anthracene (10 g, 28.654 mmol), 4,4,5,5-tetramethyl-2-(2-nitrophenyl)-1,3,2-dioxaborolane (10.7 g, 42.981mmol), K_3PO_4 (18.2g, 85.962 mmol) and s-phos (1.76 g, 4.2981 mmol) were dissolved in toluene (200 mL) and H_2O (60 mL) with degassing by nitrogen for 30 min. Tris(dibenzylideneacetone)dipalladium(0) (1.3 g, 1.4327 mmol) was added to the mixture, which was stirred for 10 h at 100 °C. After cooling to room temperature, the reaction mixture was extracted with dichloromethane. The organic layer was washed with water and then dried over $MgSO_4$. After the solvent was evaporated, the crude product was purified by column chromatography (eluent = Hexane/ dichloromethane, 6:1). After purification, the product was obtained as a solid (yield: 7.9 g, 70.4 %). ^{1}H-NMR (300 MHz, CD_2Cl_2) δ = 8.78-8.73 (m, 2H), 8.14-8.11 (m, 1H), 7.95-7.93 (d, J=8.4Hz, 1H), 7.84-7.62 (m, 6H), 7.50-7.42 (m, 3H), 7.35-7.32 (dd, J=0.8Hz, J=8.4Hz, 1H). ^{13}C NMR (500 MHz, $CDCl_3$): δ (ppm) = 160.3, 159.7, 157.7, 153.2, 149.9, 134.8, 134.6, 134.4, 133.8, 133.0, 132.9, 132.1, 128.2, 124.3, 123.2, 123.0, 118.5, 118.0, 109.2; HRMS (EI+, m/z): calcd for $C_{24}H_{14}NO_4B$ 391.1016, found 391.1019.

Synthesis of 11H-9,16-dioxa-11-aza-4b-boraindeno[1,2-a]naphtho[3,2,1-de]anthracene (4) 8-(2-Nitrophenyl)-5,9-dioxa-13b-boranaphtho[3,2,1-de]anthracene (7.0 g, 10.225 mmol) was dissolved triethylphosphite (20 mL, 112.477 mmol) under a nitrogen atmosphere. The reaction

mixture was stirred for 10 h at 160 ℃. After cooling to room temperature, the reaction mixture was extracted with dichloromethane. After cooling to room temperature, the reaction mixture was extracted with dichloromethane. The organic layer was washed with water and then dried over $MgSO_4$. After the solvent was evaporated, the crude product was purified by column chromatography (eluent = Hexane/ dichloromethane, 7:1). After purification, the product was obtained as a solid (yield: 4.5 g, 70 %). ^{1}H-NMR (300 MHz, CD_2Cl_2) δ = 8.88-8.82 (dd, J=1.3Hz, J=7.8Hz, 1H), 8.80-8.77 (dd, J=1.6Hz, J=7.7Hz, 1H), 8.70-8.67 (m, 1H), 8.63 (s, 1H), 7.91-7.82 (m, 2H), 7.79-7.73 (m, 1H), 7.61-7.42 (m, 6H), 7.33 (s, 1H). ^{13}C NMR (500 MHz, $CDCl_3$): δ (ppm) = 160.6, 160.0, 156.3, 153.1, 145.0, 139.0, 134.5, 134.4, 133.0, 132.9, 125.0, 123.0, 122.4, 122.4, 122.2, 120.7, 118.4, 118.1, 110.1, 105.9, 90.6; HRMS (EI+, m/z): calcd for $C_{24}H_{14}NO_2B$ 359.1118, found 359.1117.

Synthesis of 11-phenyl-11H-9,16-dioxa-11-aza-4b-boraindeno[1,2-a]naphtho[3,2,1-de] anthracene (5) 11H-9,16-dioxa-11-aza-4b-boraindeno[1,2-a]naphtho[3,2,1-de]anthracene (4.5 g, 12.528 mmol), K_3PO_4 (10.64 g, 50.112 mmol), CuI (0.23 g, 1.2528 mmol), I-Benzene (7.6 g, 37.584 mmol) and trans-1,2-biaminocyclohexane (0.22 g, 1.8792 mmol) were dissolved in 1,4-dioxane (100.0 mL) under a nitrogen atmosphere. The reaction mixture was stirred for 10 h at 100 ℃. After cooling to room temperature, the reaction mixture was extracted with dichloromethane. After cooling to room temperature, the reaction mixture was extracted with dichloromethane. The organic layer was washed with water and then dried over $MgSO_4$. After the solvent was evaporated, the crude product was purified by column chromatography (eluent = Hexane/ dichloromethane, 6:1). After purification, the product was obtained as a solid (yield: 2.9 g, 53.1 %). ^{1}H-NMR (300 MHz, CD_2Cl_2) δ = 8.85-8.82 (dd, J=1.5Hz, J=7.7Hz, 1H), 8.80-8.75 (m, 2H), 7.94-7.83 (m, 2H), 7.77-7.69 (m, 5H), 7.70-7.60 (m, 1H), 7.56-7.41 (m, 6H), 7.22 (s, 1H). ^{13}C NMR (500 MHz, $CDCl_3$): δ (ppm) = 160.6, 160.0, 156.3, 153.1, 146.4, 141.0, 137.2, 134.5, 134.4, 133.0, 132.9, 130.0, 128.1, 127.3, 124.9, 123.1, 122.4, 122.3, 121.1, 118.5, 118.0, 109.5, 105.7, 90.1; HRMS (EI+, m/z): calcd for $C_{30}H_{18}NO_2B$ 435.1431, found 435.1433.

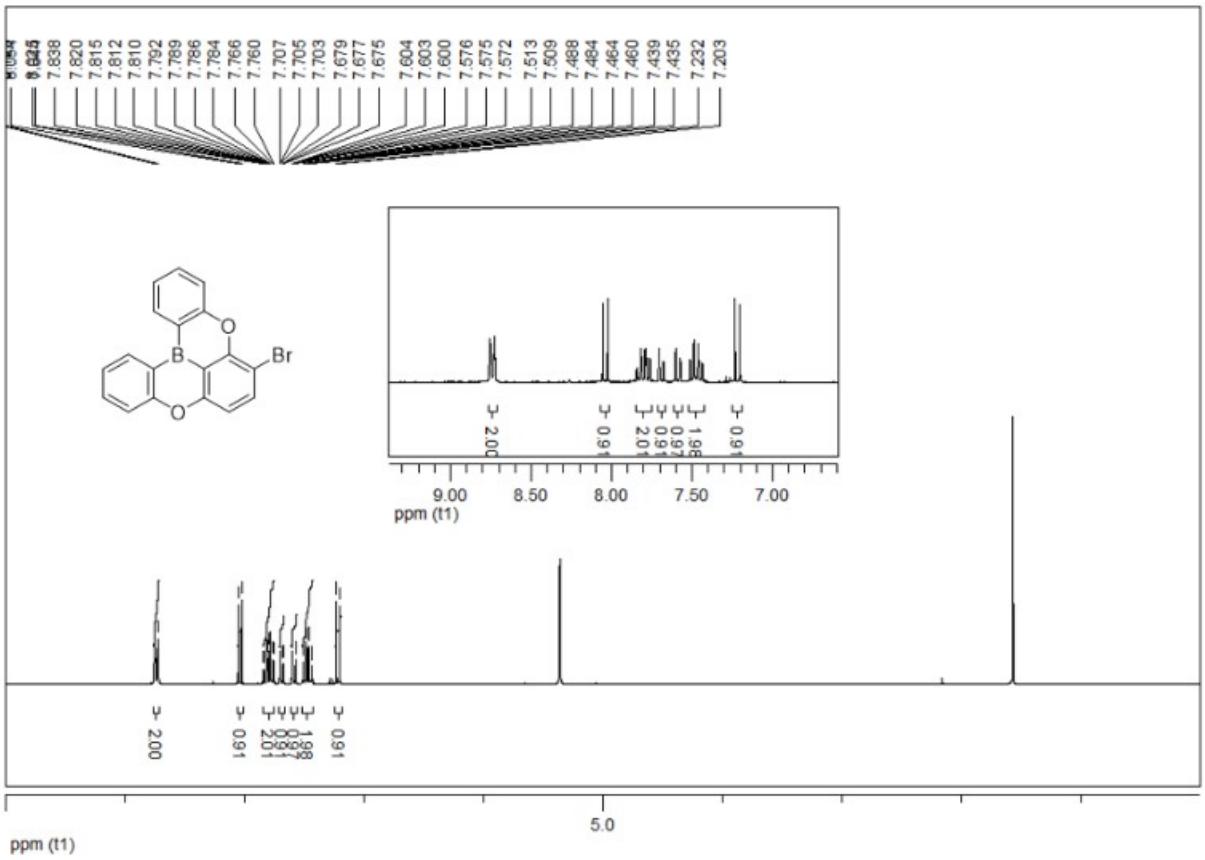

Figure S1. ^{1}H NMR data of 8-bromo-5,9-dioxa-13b-boranaphtho[3,2,1-de]anthracene (1)

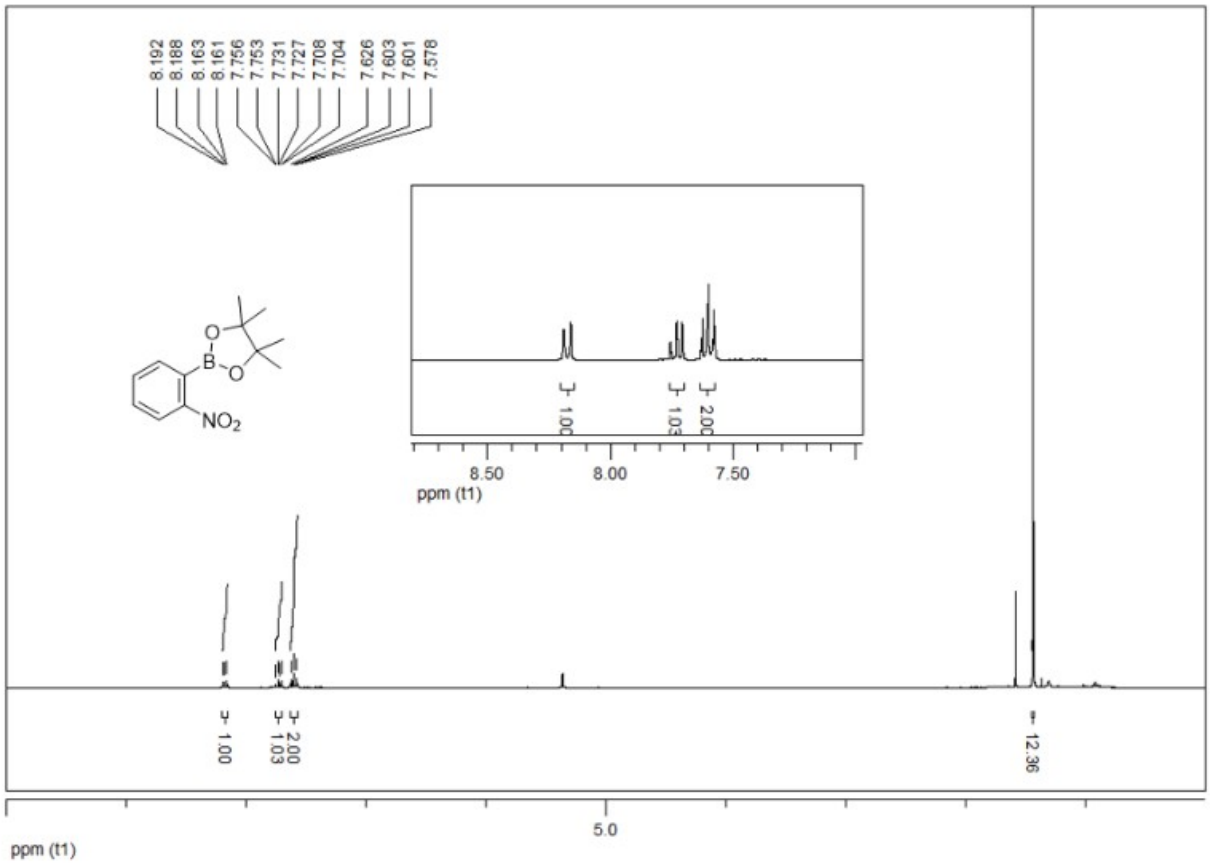

Figure S2. ^{1}H NMR data of 4,4,5,5-tetramethyl-2-(2-nitrophenyl)-1,3,2-dioxaborolane (2)

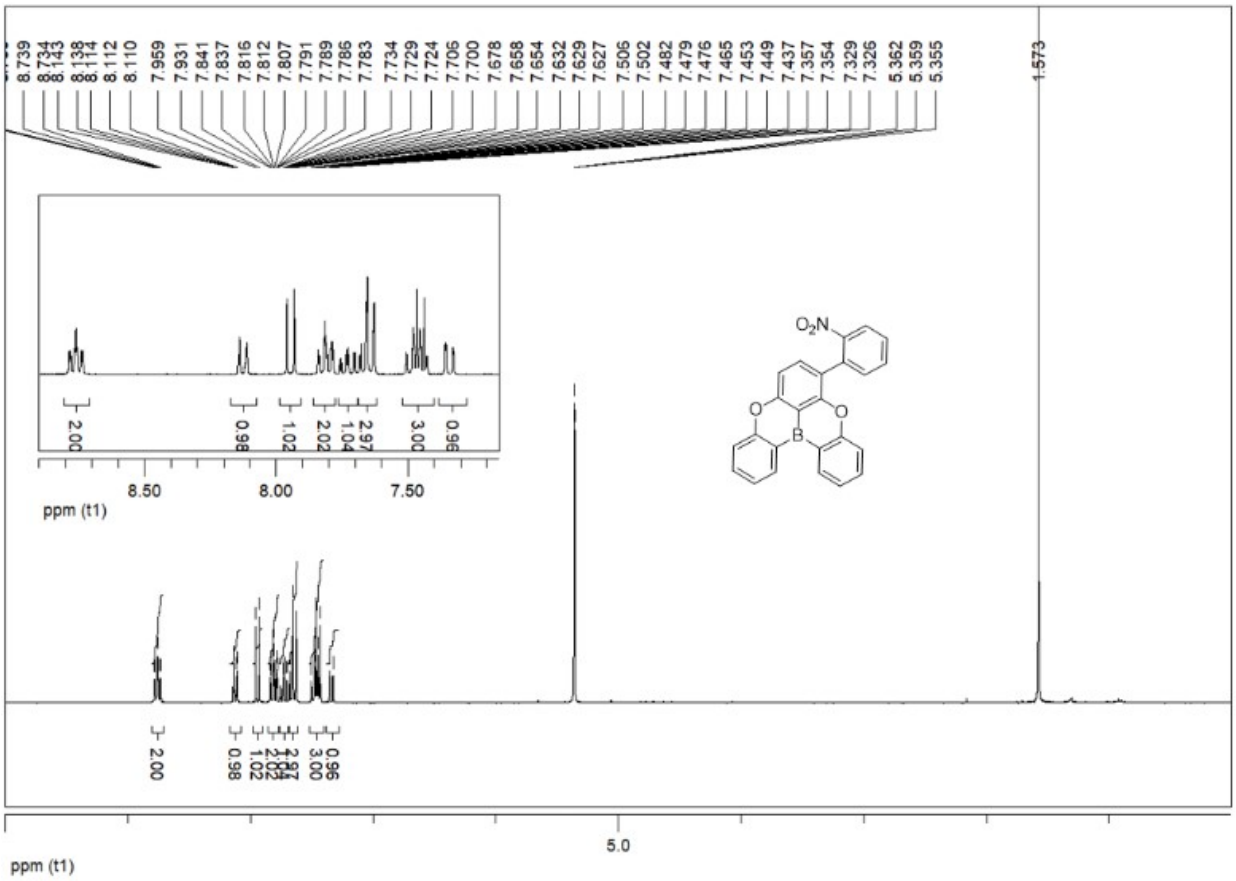

Figure S3. ^{1}H NMR data of 8-(2-nitrophenyl)-5,9-dioxa-13b-boranaphtho[3,2,1-de]anthracene (3)

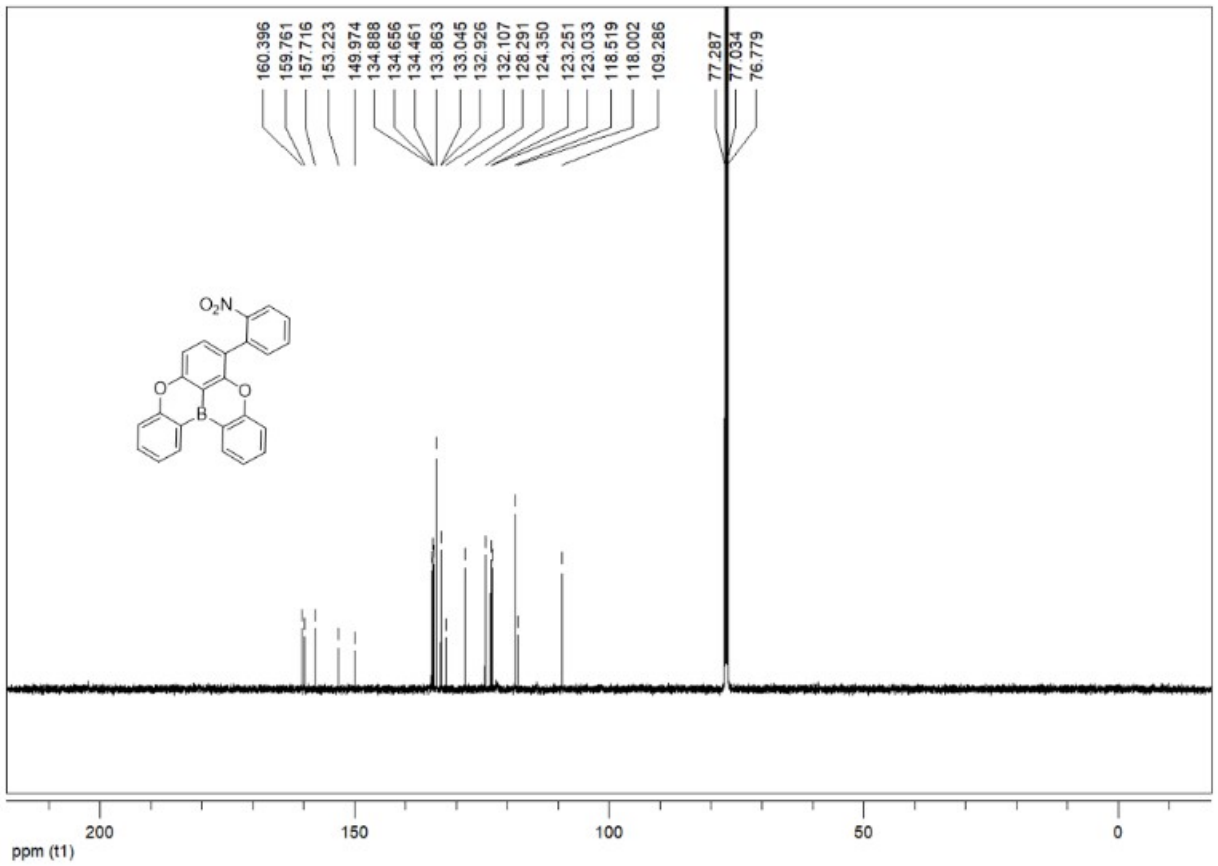

Figure S4. ^{13}C NMR data of 8-(2-nitrophenyl)-5,9-dioxa-13b-boranaphtho[3,2,1-de]anthracene (3)

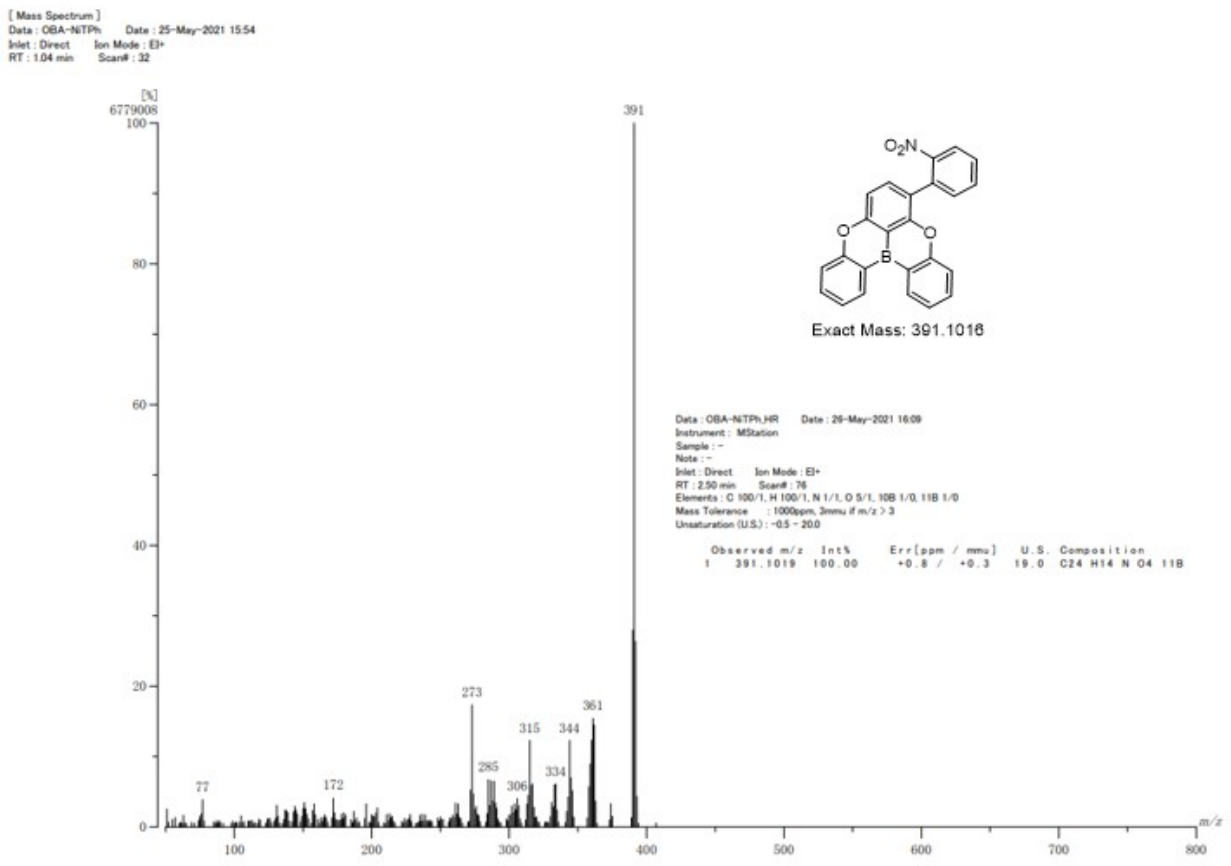

Figure S5. EI Mass data of 8-(2-nitrophenyl)-5,9-dioxa-13b-boranaphtho[3,2,1-de]anthracene (3)

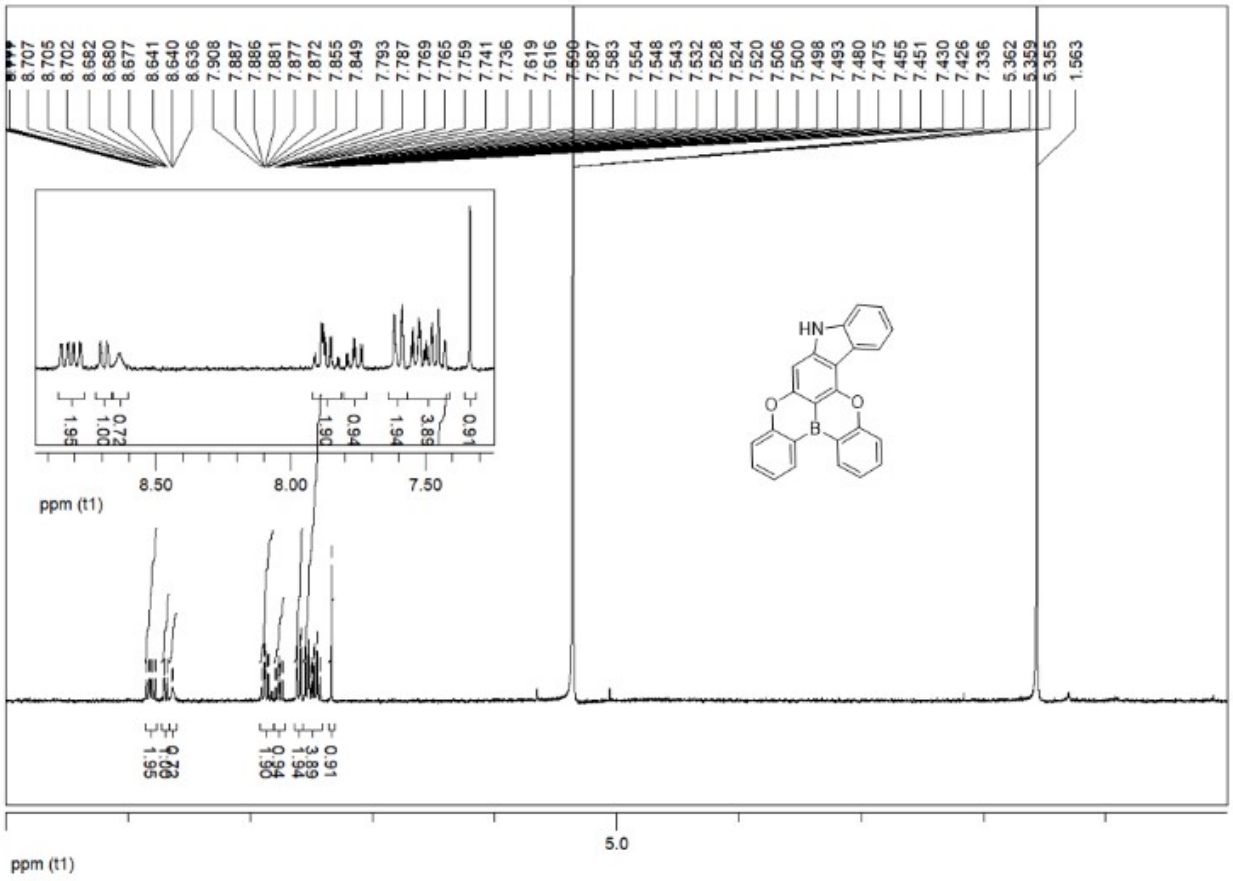

Figure S6. ^{1}H NMR data of 11H-9,16-dioxa-11-aza-4b-boraindeno[1,2-a]naphtho[3,2,1-de]anthracene (4)

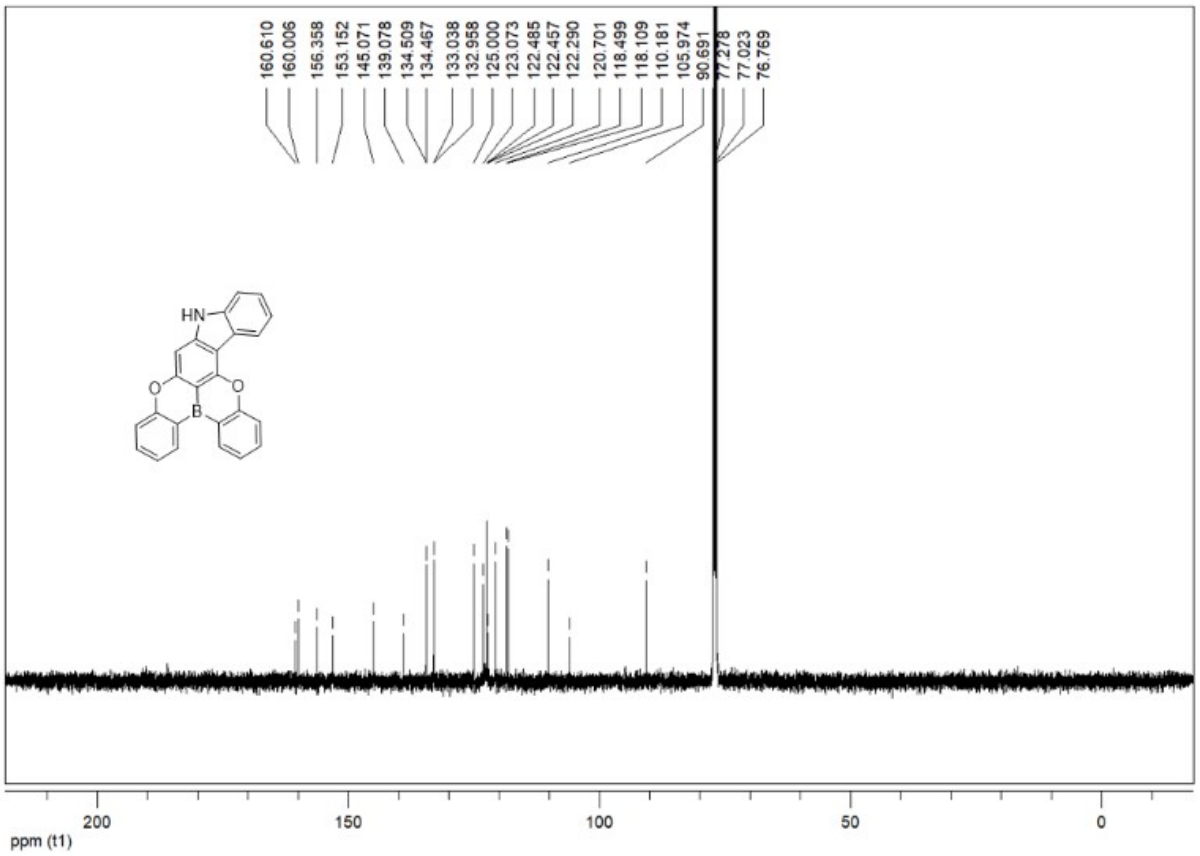

Figure S7. ^{13}C NMR data of 11H-9,16-dioxa-11-aza-4b-boraindeno[1,2-a]naphtho[3,2,1-de]anthracene (4)

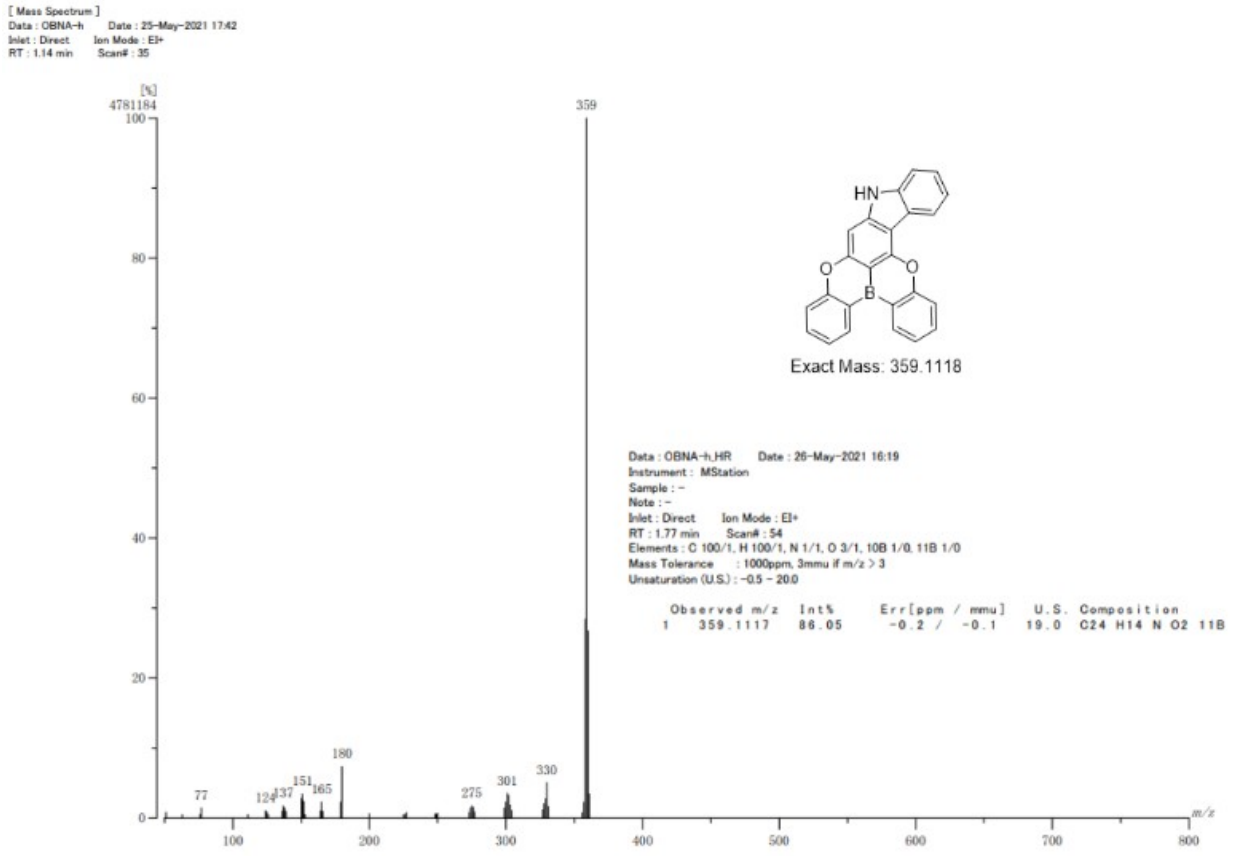

Figure S8. EI Mass data of 11H-9,16-dioxa-11-aza-4b-boraindeno[1,2-a]naphtho[3,2,1-de]anthracene (4)

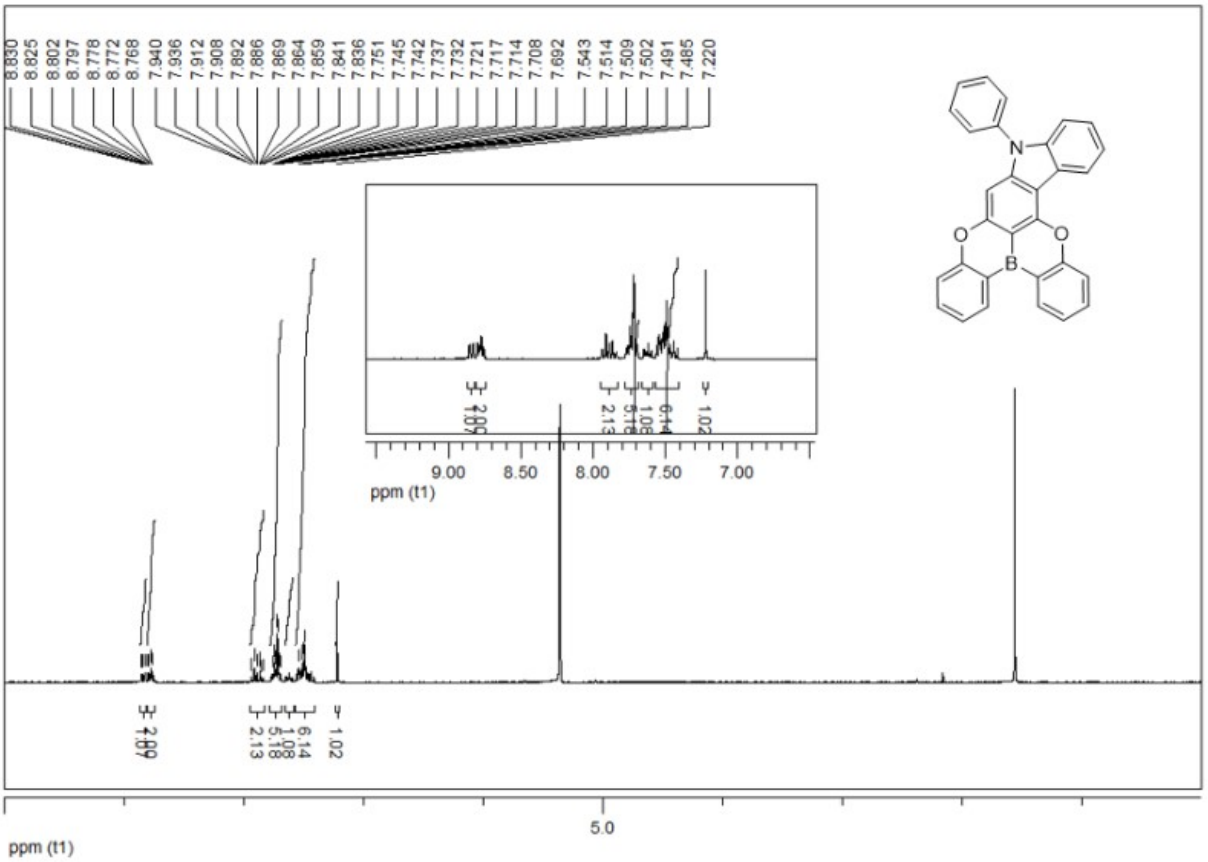

Figure S9. ^{1}H NMR data of 11-phenyl-11H-9,16-dioxa-11-aza-4b-boraindeno[1,2-a]naphtho[3,2,1-de] anthracene (5)

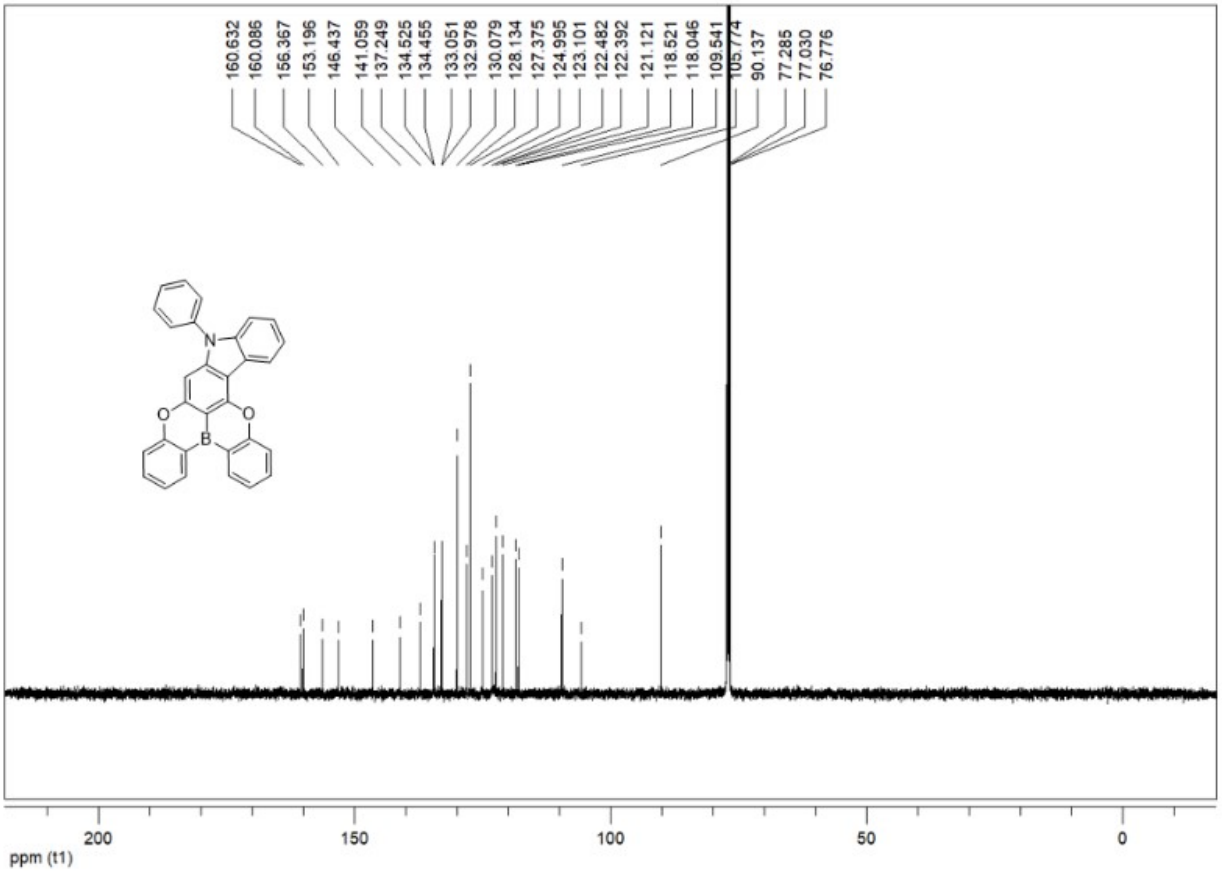

Figure S10. ^{13}C NMR data of 11-phenyl-11H-9,16-dioxa-11-aza-4b-boraindeno[1,2-a]naphtho[3,2,1-de] anthracene (5)

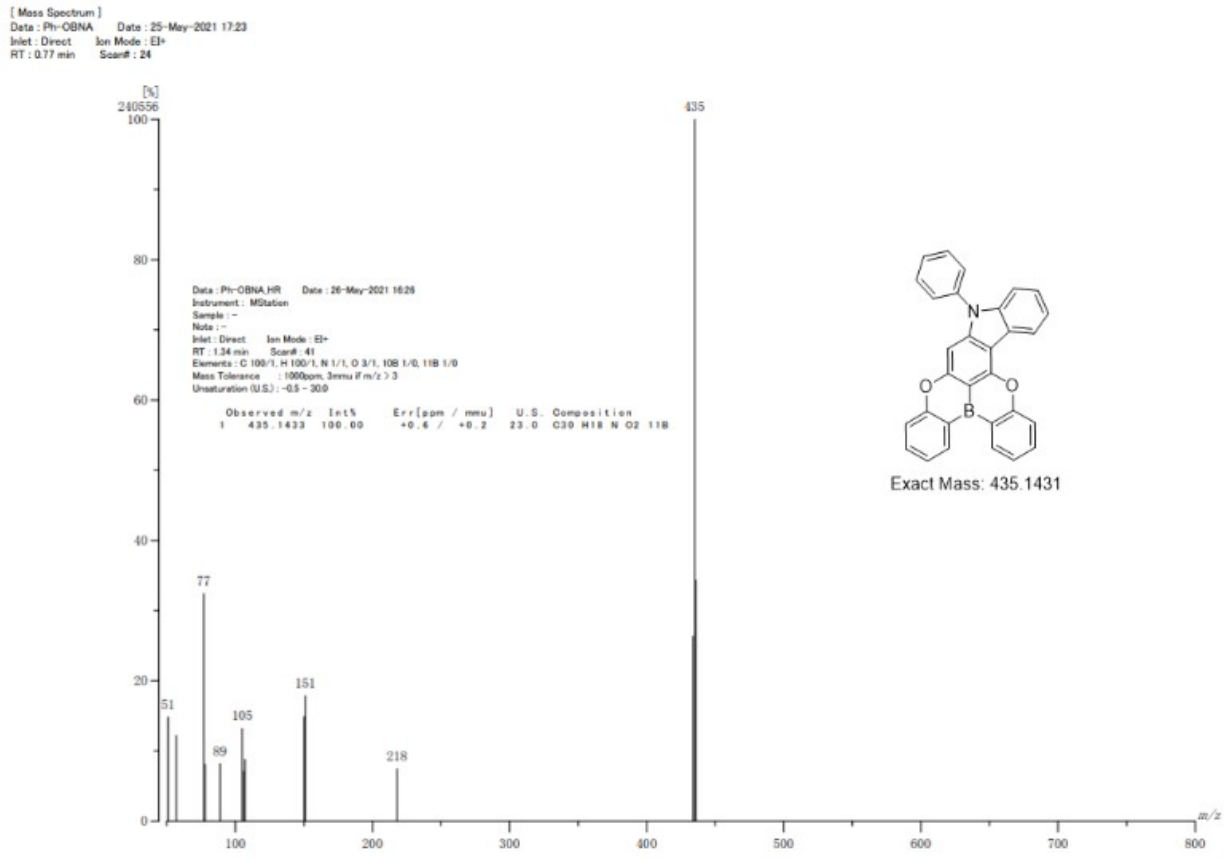

Figure S11. EI Mass data of 11-phenyl-11H-9,16-dioxa-11-aza-4b-boraindeno[1,2-a]naphtho[3,2,1-de] anthracene (5)

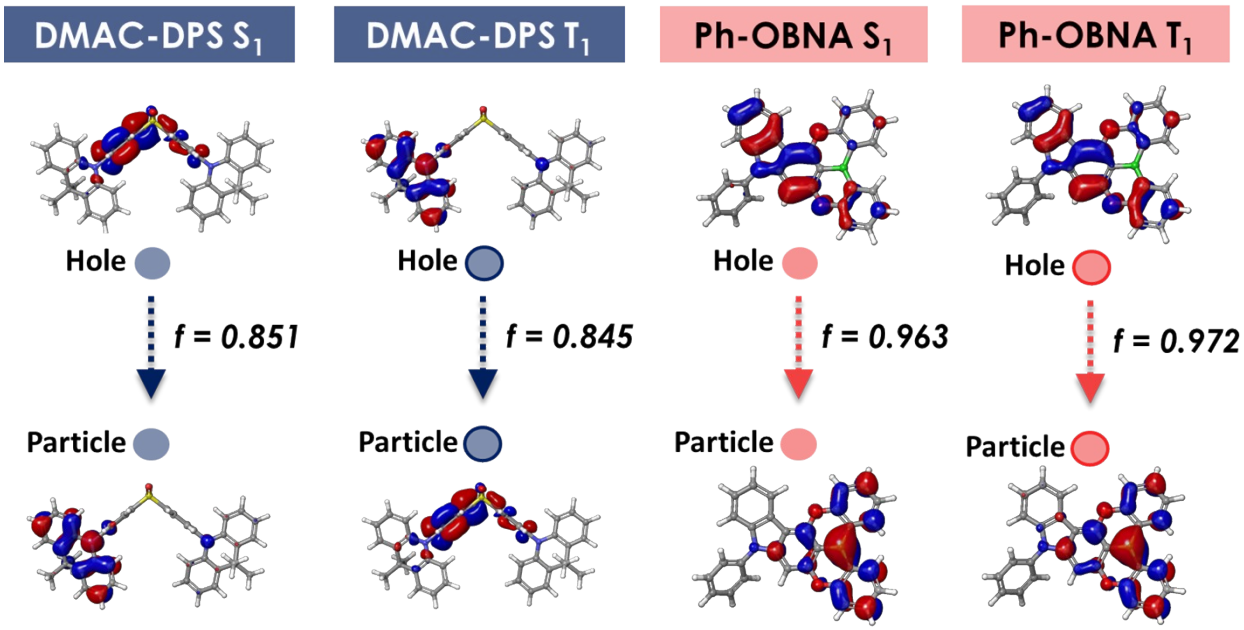

Figure S12. Natural transition orbital (NTO) analysis (a) DMAC-DPS and (b) Ph-OBNA.

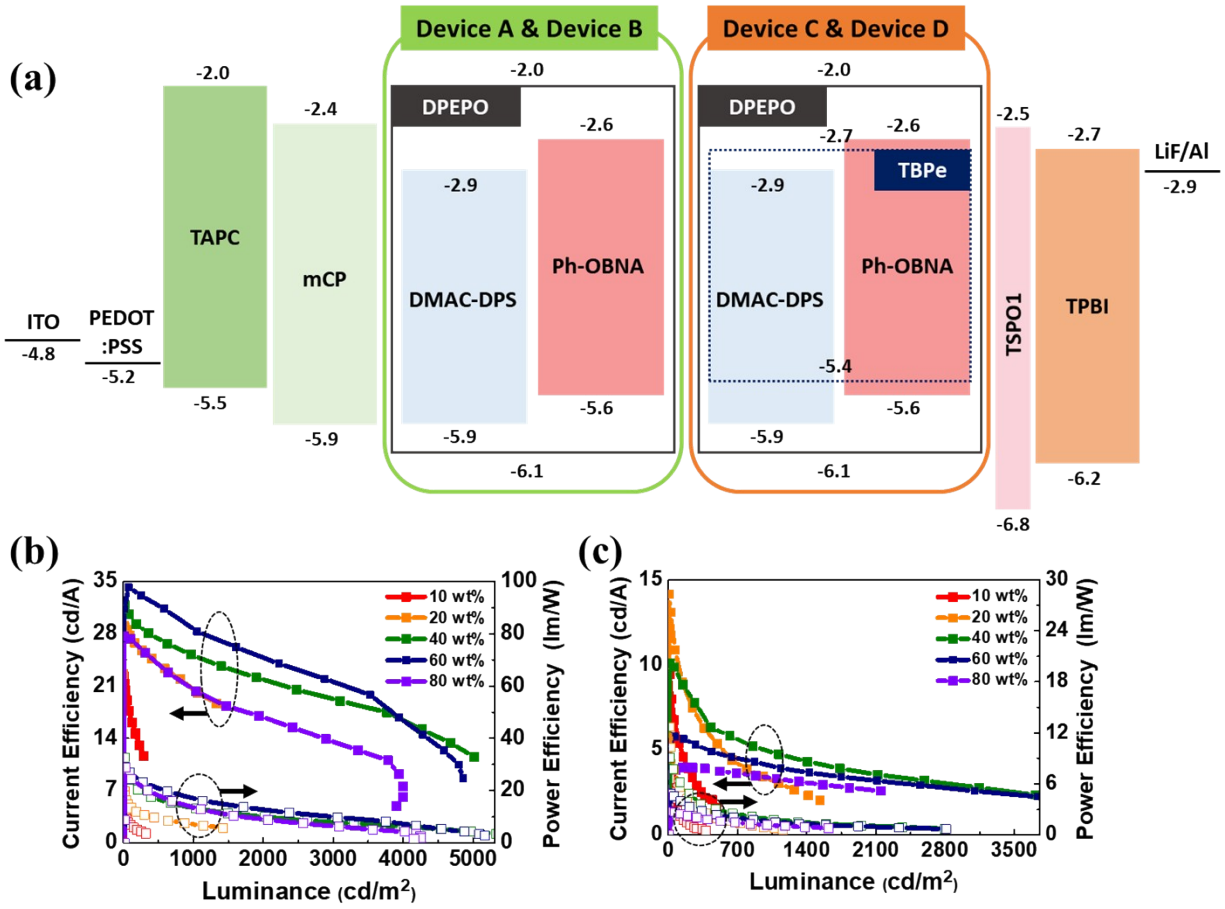

Figure S13. (a) Energy band diagram of **Device A**, **Device B**, **Device C**, and **Device D**. Current and power efficiency curves according to luminance change for (b) **Device A** and (c) **Device B**.

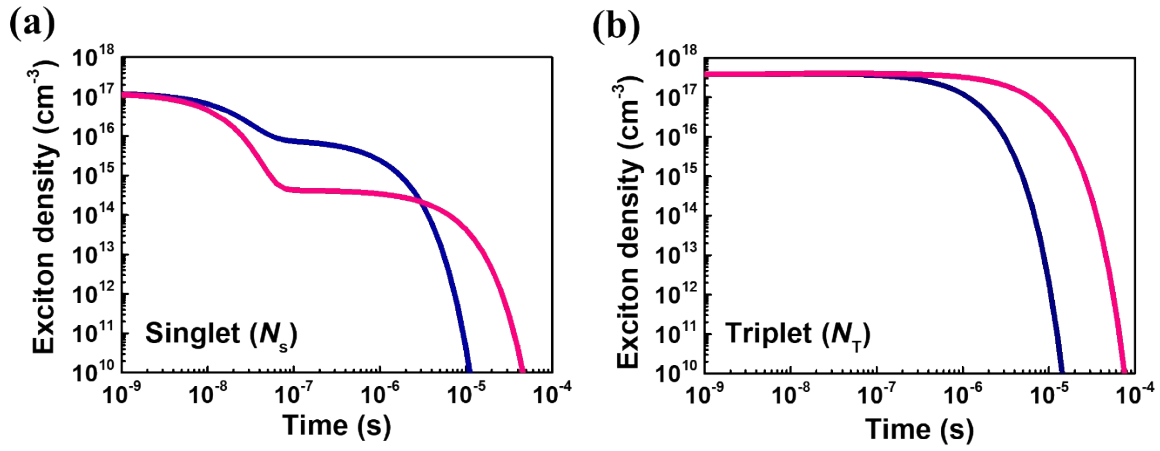

Figure S14. (a) singlet density and (b) triplet density in a DMAC-DPS (navy)/Ph-OBNA (pink):DPEPO co-deposited solid film as a function of the total time scale after electrical excitation (pulse width = 5 ns)

Table S1. Concentration quenching according to doping concentration calculated by three-level model.

20 μs	Doping concentration	τ_{PF} (ns)	τ_{DF} (μs)	k_r^S (10^6 s^{-1})	k_{RISC} (10^5 s^{-1})	k_{nr}^T (10^5 s^{-1})	k_{CQ} (10^5 s^{-1})
DMAC-DPS	10 wt%	27.2	4.29	0.68	5.38	2.23	-
	20 wt%	26.9	3.63	2.82	5.71	2.33	0.10
	40 wt%	28.9	3.12	3.70	7.86	2.37	0.14
	60 wt%	37.2	1.89	5.25	14.0	2.56	0.33
	80 wt%	30.3	2.58	8.44	11.0	1.06	-
Ph-OBNA	10 wt%	19.6	5.71	11.3	1.69	1.38	-
	20 wt%	27.4	5.58	9.30	1.08	1.52	0.14
	40 wt%	31.8	2.80	9.00	1.11	3.26	1.88
	60 wt%	38.9	2.52	8.10	0.91	3.69	2.31
	80 wt%	43.7	2.21	8.39	0.67	4.29	2.91

Table S2. TTA and STA values for DMAC-DPS and Ph-OBNA.

Materials	Doping concentration	k_{TTA} (cm^3/s)	k_{STA} (cm^3/s)
DMAC-DPS	10 wt%	8.55 X 10^{-13}	5.84 X 10^{-11}
	20 wt%	6.60 X 10^{-13}	4.30 X 10^{-11}
	40 wt%	1.06 X 10^{-12}	4.66 X 10^{-11}
	60 wt%	5.56 X 10^{-12}	1.07 X 10^{-10}
	80 wt%	5.92 X 10^{-12}	1.78 X 10^{-10}
Ph-OBNA	10 wt%	8.70 X 10^{-13}	2.62 X 10^{-10}
	20 wt%	3.56 X 10^{-13}	1.20 X 10^{-10}
	40 wt%	6.79 X 10^{-14}	1.92 X 10^{-11}
	60 wt%	1.12 X 10^{-14}	3.19 X 10^{-12}
	80 wt%	2.63 X 10^{-15}	8.99 X 10^{-13}

Reference

(1) E. Runge, E. K. U. Gross.; Density-Functional Theory for Time-Dependent Systems. *Phys. Rev.* **1984**, 52, 997.
(2) P. K. Samanta, D. Kim, V. Coropceanu, J. -L. Bredas.; Up-Conversion Intersystem Crossing Rates in Organic Emitters for Thermally Activated Delayed Fluorescence: Impact of the Nature of Singlet vs Triplet Excited States. J. Am. Chem. **2017**, 139, 4042-4051.
(3) Y. Gao, Y. Geng, Y. Wu, M. Zhang, Z. -M. Su.; Investigation on the effect of connected bridge on thermally activated delayed fluorescence property for DCBPy emitter. *Dyes and Pigments*.**2017**, 145, 277-284.
(4) T. Stein, J. Autschbach, N. Govind, L. Kronik, R. Baer.; Curvature and Frontier Orbital Energies in Density Functional Theory. *J. Phys. Chem. Lett*. **2012**, 3, 3740−374.
(5) J. Zhang, H. Yuan, S. Feng, K. Wen, X. Guo.; Theoretical studies on electroluminescent mechanism of a series of thermally activated delayed fluorescence emitters possessing asymmetric-triazine-cored triads. *SAA.* **2018**, 202, 102-106.
(6) R.A. Marcus.; On the Theory of Oxidation-Reduction Reactions Involving Electron Transfer. I. *J. Chem. Phys.* **1956**, 24, 966.
(7) R.A. Marcus.; N. Sutin. Electron transfers in chemistry and biology. *BBA*, **1985**, 811, 265-322.
(8) F. Wang, T. Ziegler.; The calculation of excitation energies based on the relativistic two-component zeroth-order regular approximation and time-dependent density-functional with full use of symmetry. *J. Chem. Phys.* **2005**, 122, 204103.
(9) E. Y. -T. Li, T. -Y. Jiang, Y. Chi, P. -T. Chou., Semi-quantitative assessment of the intersystem crossing rate: an extension of the El-Sayed rule to the emissive transition metal complexes. *Phys. Chem. Chem. Phys*. **2014**, 16, 26184.
(10) J. P. Perdew, K Burke, M. Ernzerhof, *Phys. Rev. Lett.* **1996**, 77, 3865.
(11) H. Kaji, H. Suzuki, T. Fukushima, K. Shizu, K. Suzuki, S. Kybo, T. Komino, H. Oiwa, F. Suzuki, A. Wakamiya, Y. Murata, C. Adachi.; Purely organic electroluminescent material realizing 100% conversion from electricity to light. Nat. Commun. **2015**, 6, 8476.
(12) Y. Wada, H. Nakagawa, S. Matsumoto, Y. Wakisaka, H. Kaji.; Organic light emitters exhibiting very fast reverse intersystem crossing. *Nat. Photonics*. **2020**, 14, 643-649.
(13) H. S. Kim, S. -R. Park, M. C. Suh., Concentration quenching behavior of thermally activated delayed fluorescence in a solid film. *J. Phys. Chem. C.* **2017**, 121, 13986-13997.
(14) D. Song, Y. Yu, D. Yue, Y. Zhang, X. Yang, Y. Sun, G. Zhou, Z Wu., Asymmetric thermally activated delayed fluorescence (TADF) emitters with 5,9-dioxa-13b-boranaphtho[3,2,1-de]anthracene (OBA) as the acceptor and highly efficient blue-emitting OLEDs. *J. Mater. Chem*. C. **2019**, 7(38) 11953-11963.
(15) O. Baudoin, D. Guenard, F Gueritte., Palladium-Catalyzed Borylation of Ortho-Substituted Phenyl Halides and Application to the One-Pot Synthesis of 2,2‘-Disubstituted Biphenyls. *Org. Chem.* **2000**, 65(26) 9268-9271.